ARTICLE

Check for updates

Northeast Pacific marine heatwaves linked to Kuroshio Extension variability

E. Nishchitha S. Silva [1✉] & Bruce T. Anderson [1]

Marine heatwave events in the Northeast Pacific Ocean from 2013-2015 and 2019-2020 have had significant impacts on ocean life and livelihoods in the region. Numerous studies have linked these marine heatwaves to known modes of climate variability. Here we show that the observed evolution of the 2013-2015 Northeast Pacific marine heatwave best correlates with the evolution of historical sea surface temperatures in response to variations in the Kuroshio Extension. By using ocean and atmospheric reanalysis data from 1981-2020 and ocean nutrient data from 1993-2020 from an ocean biogeochemistry model, we further report the physical and biogeochemical changes during this heat event and their relation to these same Kuroshio variations. Using these results, we propose an atmospheric teleconnection between Kuroshio Extension variations and Marine Heatwaves in the Northeast Pacific. This teleconnection's influence further extends to the marine biogeochemistry and productivity in the Northeast Pacific region via Kuroshio-influenced modifications to mixed layer thickness.

[1] Department of Earth and Environment, Boston University, Boston, MA, USA. ✉email: netige@bu.edu

Anomalous heat signatures in the ocean for prolonged periods are termed marine heatwaves (MHWs)[1,2]. An accepted definition for an MHW is a warm event with a temperature warmer than the 90th percentile of the climatological value that lasts for 5 or more days[3]. Such heat events for prolonged periods can cause devastating changes in the marine environment[4-10]. From 1925 to 2015 global average frequency of MHWs increased by 34% and lasted 17% longer[11], exposing marine environments to species range shifts, local extinctions, and coral bleaching[1,3,4,12] thus making biodiversity as well as fisheries, seafood, and aquaculture industries more vulnerable[13].

A prime example occurred from 2013 to 2015 when the Gulf of Alaska region in the Northeastern Pacific Ocean faced anomalously high sea surface temperature levels (Fig. 1). This event was later termed The Blob[9]. A prominent incident in the history of MHWs, the Blob made drastic modifications to ecosystem dynamics and productivity in the region[14]. These included low primary productivity[15], starvation of red abalone (Haliotis rufescens) populations[16], population collapse of a keystone predator (Pycnopodia helianthoides)[17], latitudinal shifts of coastal biota to the northern parts of the California Current's shelf/slope region[18-20], mass mortalities of sea birds along the Pacific Northwest beaches[21], large whale mortalities in the Gulf of Alaska[22,23] and California Sea Lion mortalities[24]. The negative socioeconomic impacts of the Blob worsened due to the occurrence of a harmful algal bloom that prompted the prolonged closure of shellfish fishing industries in the states of Washington, Oregon, and California[25]. Further, the Pacific Cod fishery was impacted negatively as a result of the Blob[26]. Importantly these ecosystem effects can persist long after the MHW dissipates[27]. In addition, in 2019, scientists saw a reemergence of the Blob in the region[28], which could potentially aggravate the ecosystem effects from the earlier MHW.

Numerous studies have attempted to explain what caused the Blob and its implications[9,15,27,29-31]. The resilient extreme warm ocean anomaly observed during the Blob was initially a result of a ridge, or high-pressure anomaly, on the eastern side of the Blob, which has been termed a "Ridiculously Resilient Ridge"[32]. Hypotheses that explain the resiliency of this ridge include remote teleconnections driven by warmer than normal western North Pacific[33,34]; the influence of Arctic Sea ice loss on the North Pacific geopotential height fields[35]; and atmospheric internal variability[36]. Further research on the persistence of this atmospheric anomaly and its influence on marine climate extremes also highlights the role of known modes of decadal climate variability. For instance, both the Pacific Decadal Oscillation[37]

and the North Pacific Gyre Oscillation[38] have been hypothesized to sustain marine heatwaves in the Gulf of Alaska[2,29,31,39]. However, a new mode of quasi-decadal variability over the tropical and extratropical North Pacific—the Pacific Decadal Precession (PDP)—has been revealed by a 2016 study[40]. PDP, a counterclockwise progression of a mid-latitude North Pacific centered pressure dipole consisting of a north–south phase (which maps onto the North Pacific Oscillation) and an east–west phase (which maps onto the Circumglobal Teleconnection Pattern), has shown a connection with warming signals[41] in the Northeast Pacific Ocean as well as the Northeast U.S continental shelf region, two regions that suffered from MHWs during the last decade. Empirical analysis has confirmed that PDP both forces and responds to variations in the Kuroshio Extension (KE), the westward extension of the North Pacific western boundary current Kuroshio[41]. This coupled variability occurs on decadal timescales and has been termed the Ebessan Pacific Precession[41]. The Ebessan Pacific Precession comprises three stages (Fig. 2): a teleconnection stage, a tethered stage, and a tunneling stage. The teleconnection stage, where KE heat flux anomalies modify the atmospheric pressure anomalies over the North Pacific, is the stage of interest in the current study. Indeed, a robust link between KE variations and the PDP has been discovered in a recent study[42]. This study indicates that it is neither mesoscale nor the leading mode of large-scale variations of the KE that sets up a PDP-like atmospheric structure. Instead, it is the second mode of large-scale variations in the KE (a mode related to the intensification of the KE resulting from a strengthening of the meridional sea surface temperature gradient) that sets up a PDP-like north–south pressure dipole over the North Pacific which further supports a downstream high-pressure system that gives rise to the east–west phase of the PDP.

The above-mentioned link between PDP and marine heat extremes, as well as the link between KE variations and PDP, led us to investigate whether there is a link between the occurrence of MHWs in the Northeast Pacific and the variations in KE. If true, then we hypothesize that variations in the KE region will influence the marine environment in the Northeast Pacific. Indeed, the results we present in this study reveal that the observed evolution of the 2013–2015 marine heatwave in the Gulf of Alaska (GOA) (i.e., the Pacific Blob) best correlates with the lead-lag regression patterns of historical GOA SSTs to large-scale variations in the KE region. Further, the KE variations match well with the observed weakened wind stress, reduced mixed layer thickness in the GOA, and eventual reduction of primary production in the region during the period 2013–2015.
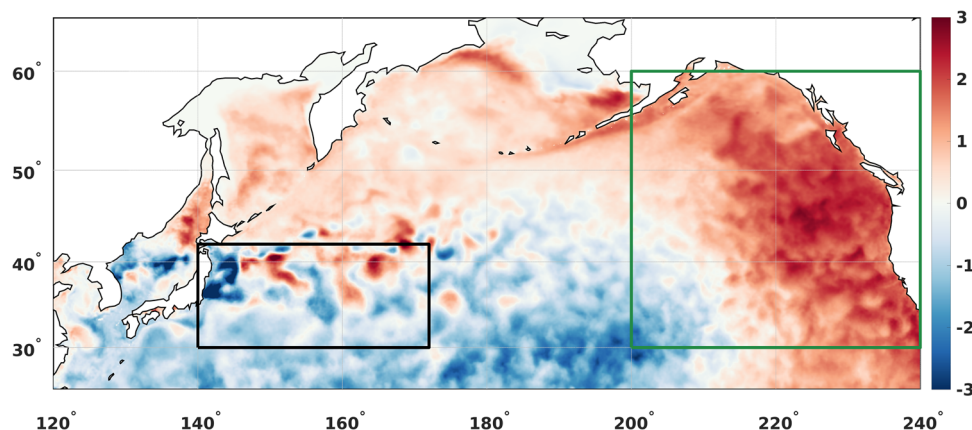

Fig. 1 Sea surface temperature anomalies during the Blob. SST anomalies of the North Pacific Ocean (shading—Units: K) for the period of February to March in the year 2015. The black box indicates the domain utilized for the development of Kuroshio Extension's large-scale index. The green box indicates the domain of the Blob occurred in the Northeast Pacific Ocean/Gulf of Alaska considered in the study.
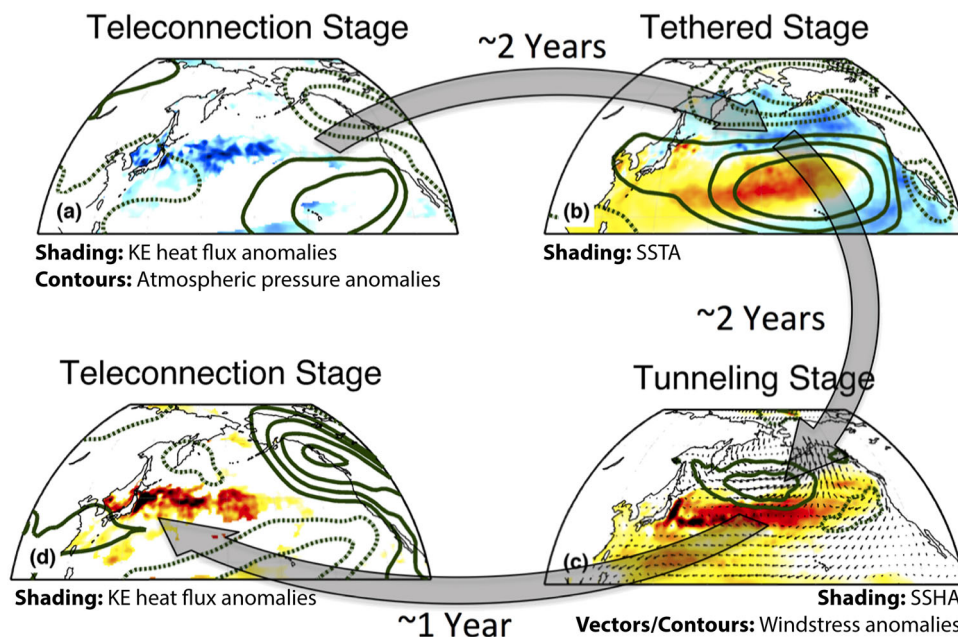
Fig. 2 Kuroshio Extension influence on the Pacific Decadal Precession. Schematic diagram showing the stages of a self-sustaining, oscillatory mode of decadal variability over the extratropical North Pacific revealed by the PDP-related diagnostics in Anderson (2019)[41]. **a** The teleconnection stage in which KE heat flux anomalies (shading) induce teleconnected atmospheric pressure anomalies (contours) over the eastern North Pacific (only showing negative heat flux anomalies). **b** The tethered stage in which sea surface temperature anomalies (SSTA) (shading) and atmospheric pressure anomalies intensify and migrate westward through unstable air-sea interactions. **c** The tunneling stage, in which PDP-related wind stress anomalies (contours; vectors) induce sea surface height anomalies (SSHA) (shading) characteristic of a first-baroclinic-mode Rossby wave (only showing positive SSH anomalies, along with wind stress vectors). **d** The teleconnection stage of the opposite sign, in which the arrival of the Rossby wave generates sea surface temperature and heat flux anomalies in the KE (only showing positive heat flux anomalies). Included from Anderson (2019)[41] with permission.
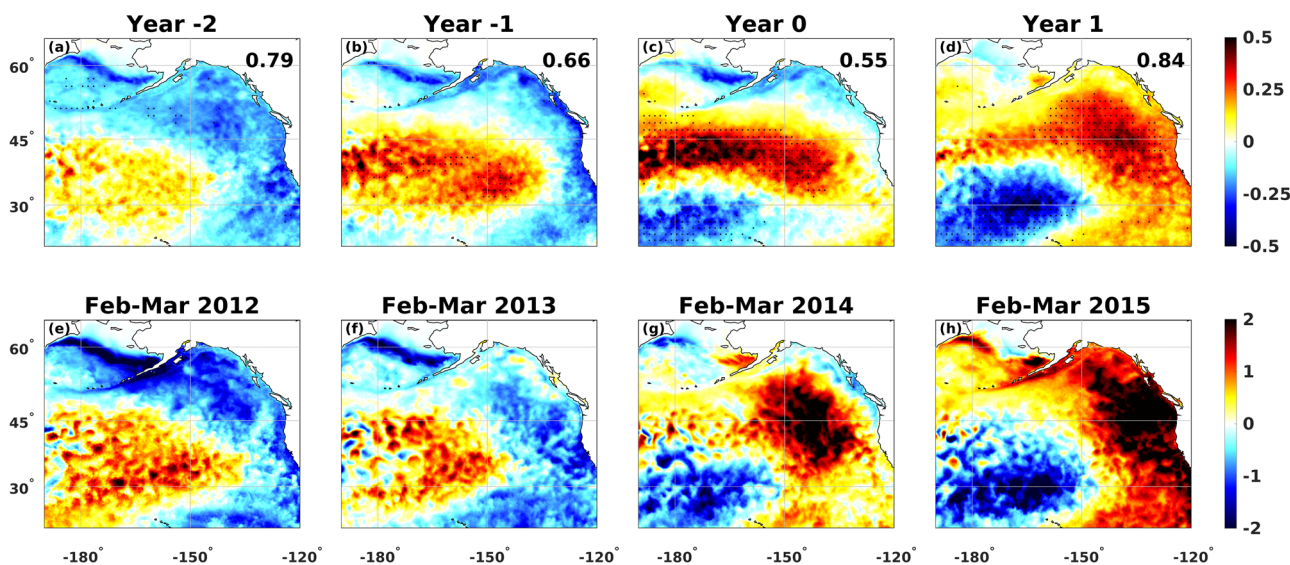

Fig. 3 Observed and KE-influenced SST anomalies. a–d Regression coefficients of sea surface temperature anomalies (shading—Units: K) when February–March SST anomalies are regressed onto the KE index—see "Methods." Positive (negative) lags indicate that the field lags (leads) the KE index. **e–h** Observed SST anomalies (shading—Units: K) in the Gulf of Alaska region from February to March of 2012–2015. The top right digit of panels **a–d** indicates the spatial correlation coefficient between regression coefficients and the corresponding Blob-related map below each regression map. Dotted shading designates regression coefficients that exceed the $p < 0.05$ value—see "Methods".

Results

KE variations and the Blob. A lead-lag regression of the SSTs in the GOA (see "Methods") on the KE index (Fig. 3) highlights that the KE-related evolution of SSTs in the Northeast Pacific well matches the evolution of the Blob in the region from 2013 to 2015. The year-to-year movement of the warm water anomaly from the west to the eastern portion of the domain can be seen in both lead-lag evolution maps (Fig. 3a–d) and the observed SST evolution (Fig. 3e–h). From lag Year −2 to Year 1, the spatial correlation between the regression coefficients and observed SST changes is strong. This provides evidence that the evolution of SSTs in the GOA region during the Blob is influenced by KE variations both intra-seasonally and inter-annually. To further confirm this influence of the KE variations, we obtained the
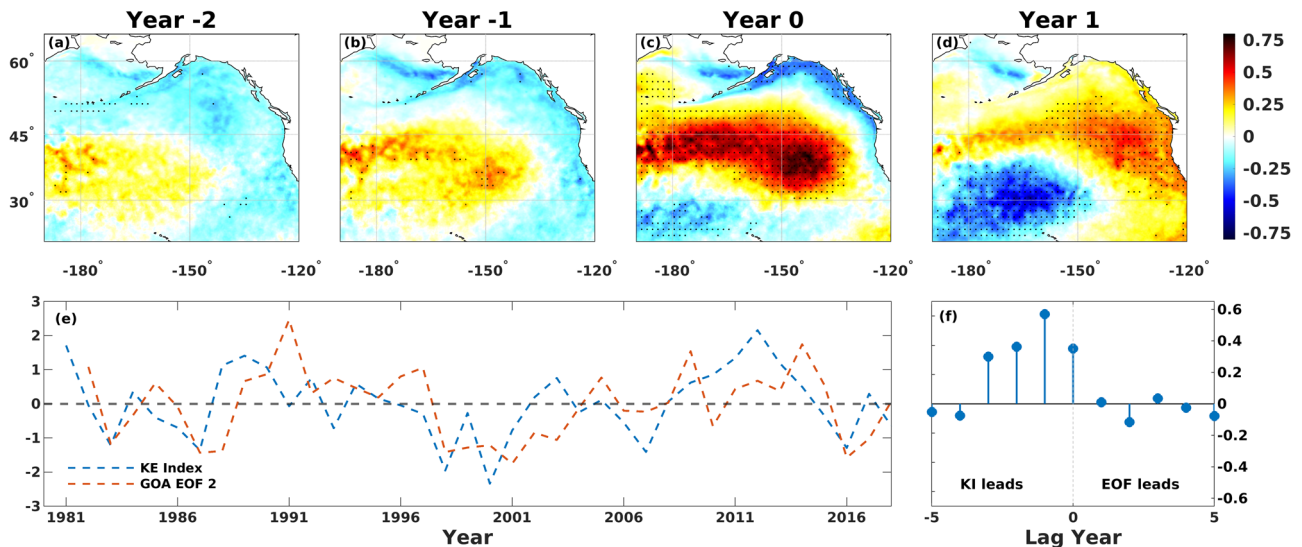
Fig. 4 SST variability in the Gulf of Alaska region. a–d Regression coefficients of sea surface temperature anomalies (shading—Units: K) when 2nd February–March SST anomalies were regressed on the Gulf of Alaska 2nd EOF time-series. Positive (negative) lags indicate that the field lags (leads) EOF time series. Dotted shading designates regression coefficients that exceed the $p < 0.05$ value—see "Methods." **e** A comparison between KE index and Gulf of Alaska 2nd EOF time-series. **f** Lead-lag correlation analysis output between KE index and Gulf of Alaska 2nd EOF time-series.
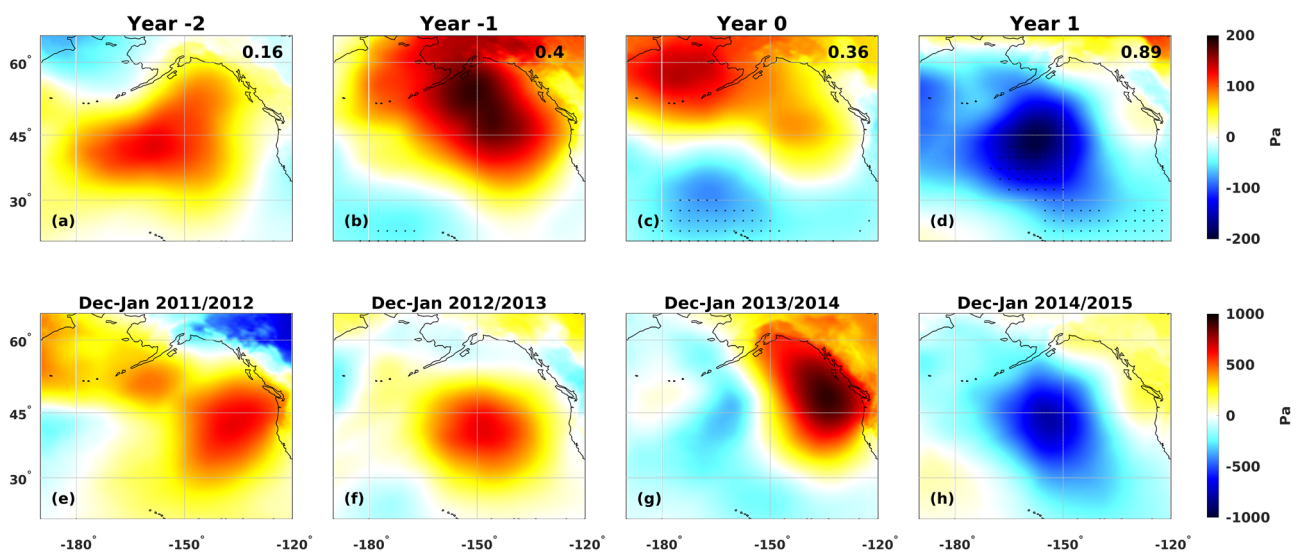

Fig. 5 KE influenced and observed SLP anomalies. Same as Fig. 3 except for **a–d** lag regression coefficients of December–January SLP anomalies (shading—Units: Pa). **e–h** Observed SLP anomalies (shading—Units: Pa) for December to January 2012 to 2015 The top right digit of panels **a–d** indicates the spatial correlation coefficient between regression coefficients and the corresponding Blob-related map below each regression map. Dotted shading designates regression coefficients that exceed the $p < 0.05$ value—see "Methods".

leading modes of SST variability in the GOA. When the GOA SSTs were regressed on the second EOF of GOA variability time-series (Fig. 4a–d), it also matched with the Blob evolution. Further, the KE index and GOA 2nd EOF time series (Fig. 4e) have a notable correlation when the GOA EOF time series is lagged by 1 year ($R^2 = 0.6$) (Fig. 4f).

What links the KE and the Blob? To determine the teleconnection between KE variations and the Blob via the atmosphere, we first investigated the lead-lag influence of KE variations on sea level pressure (SLP) (Fig. 5a–d) and whether this influence is consistent with the evolution of the December and January SLP during the Blob (Fig. 5e–h). The higher-than-normal SLP anomaly observed from October 2012 to February 2013—noted by previous investigations and discussed above[9] is also

present in our analysis. This high-pressure anomaly is followed by a lower-than-normal SLP anomaly arriving from the central North Pacific towards the GOA the next year. The systematic evolution of the low-pressure system is supported by a 2-year-long analysis (See Supplementary Fig. 1). When looking at the KE-influenced SLP evolution, we see the same kind of low-pressure system arriving from the central North Pacific towards the GOA starting in 2014 and persisting into 2015 (Fig. 5d). Dynamic links between the KE variations and these SLP modifications can be explained using prevailing works[41–43]. Particularly, the second mode of the large-scale KE variations induces specific atmospheric and oceanic patterns by warming (cooling) of the ocean in the southern (northern) region of the KE. This temperature anomaly sets up a north–south atmospheric pressure dipole over the North Pacific Ocean. The altered large-scale
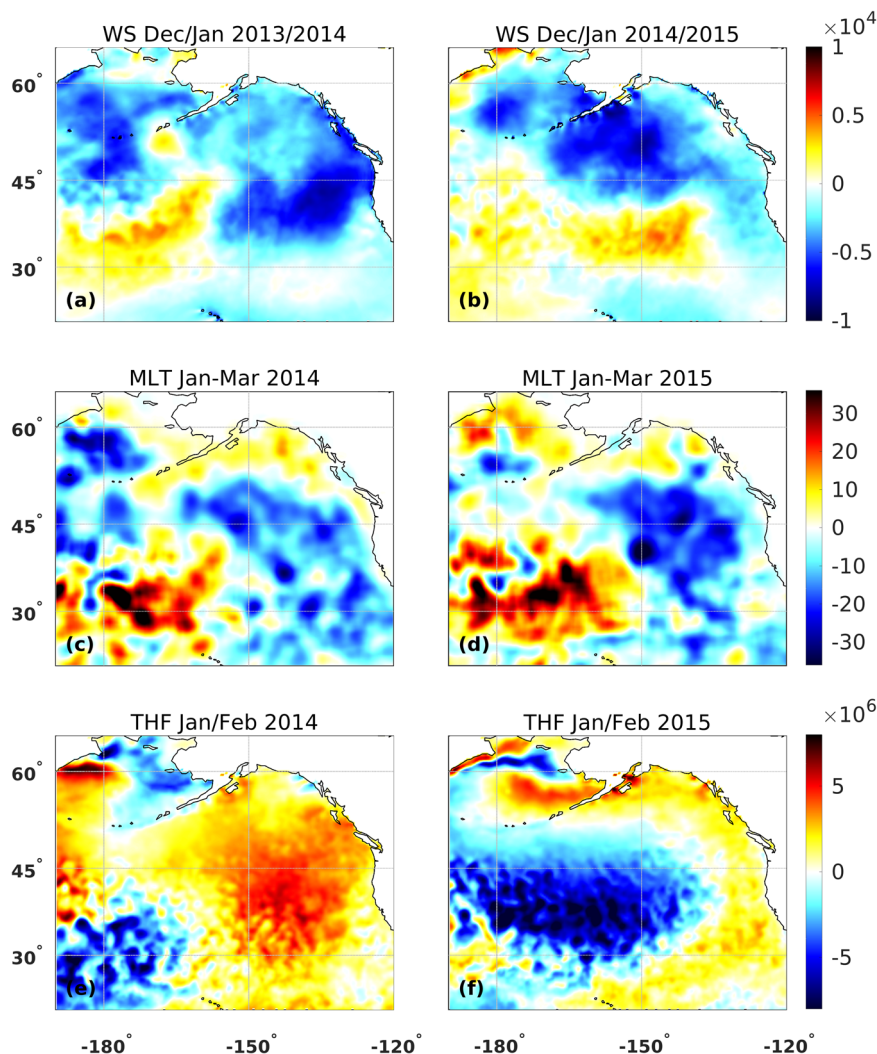
Fig. 6 Observed ocean dynamics. a, b Observed turbulent surface stress anomalies (WS) in the Gulf of Alaska region from 2013 to 2015 winters (shading —Units: Nm^{-2} s). **c, d** Observed mixed layer thickness (MLT) in the Gulf of Alaska region from 2013 to 2015 winters (shading—Units: m). **e, f** Observed total heat flux (THF) in the Gulf of Alaska region from 2013 to 2015 winters (shading—Units: Jm^{-2} and the convention is positive downward).

baroclinicity of the atmosphere and the zonal intensification of a straight jet contribute to this dipole formation, thus affecting the zonal propagation of stationary wave energy, leading to a reduction in its eastward movement. Additionally, it enhances the climatological zonal wave heights over North America. Consequently, a downstream response occurs over the North American continent, along with the formation of an east–west pressure dipole over the North Pacific and North American regions. This process has been both dynamically and empirically analyzed by Silva & Anderson[42].

To understand the role the changing SLP field plays in initiating and sustaining the Blob, we next analyze turbulent wind stress, ocean mixed layer thickness, and surface heat fluxes and how their evolution matches the observed spatial patterns during the Blob (Fig. 6). We selected December to January months for turbulent wind stress, January to March months for mixed layer thickness, and January to February for total heat flux based upon the seasonal climatology (see "Methods"). November to December KE variations relate to a weakened windstress in the GOA region (Fig. 7a). This influence remains for another year, especially within the Blob region (Fig. 7b) (See Supplementary Fig. 2). The KE-related windstress patterns spatially correlate well with the observed windstress patterns during the Blob.

Turning to the mixed layer thickness, it too was reduced as a result of KE's influence from Year 0 to Year 1, again showing a very strong spatial correlation with the evolution of the Blob patterns (Fig. 7c, d). Finally, in year 0, KE results in an anomalous surface energy flux into the GOA region, and in year 1, the surface energy flux into the ocean can be seen extending southward along the western coast of the continent (Fig. 7e, f). These spatially match with the observed energy fluxes during the Blob. Taken together, these results suggest that the KE-related changes in SLP weaken the wind stress over the GOA region, which in turn diminishes the mixed layer thickness, which would support the enhanced sea surface temperature anomalies associated with the Blob. Further in Year 0, the reduced wind stress reduces the ocean heat flux from the ocean to the atmosphere, which would further amplify the sea surface temperature anomalies; however, during Year 1, the sign of the heat flux anomalies reverses sign, indicating enhanced heat flux from the ocean to the atmosphere, which would tend to dampen the sea surface temperature anomalies, not enhance them.

Influence of KE on the marine environment. Above, we analyzed the KE's influence on the physical marine environment. At the same time, it also has an influence on the biochemical
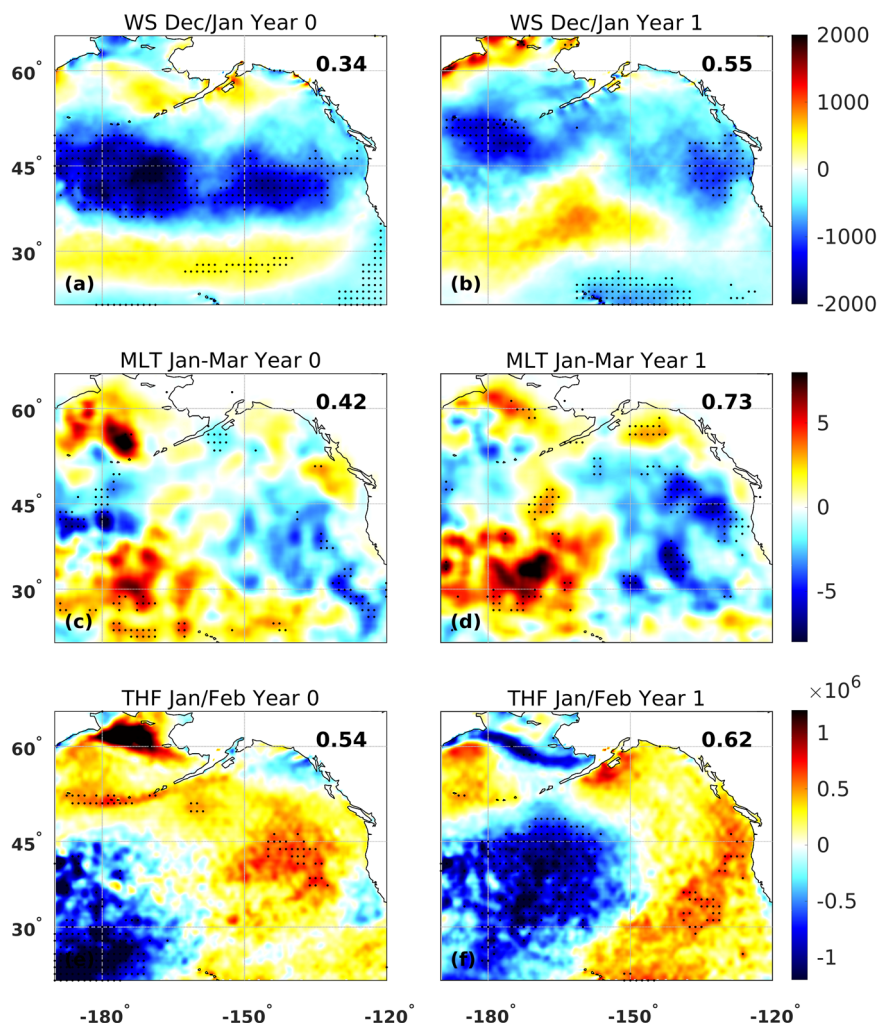
Fig. 7 KE-influenced ocean dynamics. a, b Regression coefficients of turbulent surface stress anomalies (WS) (shading—Units: Nm^{-2} s) when Dec–Jan WS is regressed on KE index with no lag, and WS lagged by 1 year, respectively. **c, d** Regression coefficients of mixed layer thickness (MLT) (shading—Units: Nm^{-2} s) when Jan–Mar MLT is regressed on the KE index with no lag and MLT lagged by 1 year, respectively. **e, f** Regression coefficients of total heat flux (THF) (shading—Units: Jm^{-2}) when Jan–Feb THF is regressed on the KE index with no lag, and THF lagged by 1 year, respectively. The top right digit of each panel indicates the spatial correlation coefficient between regression coefficients and the corresponding Blob-related map panel from Fig. 6. Dotted shading designates regression coefficients that exceed the $p < 0.05$ value—see "Methods".

environment in the GOA. Prevailing literature suggests that reduced windstress and mixed layer depths can reduce nutrient replenishment in the Gulf of Alaska region[44]. During the Blob years, nutrient availability and the primary productivity in the GOA region were indeed reduced (Fig. 8). We link this to the declined mixed layer thickness in the region because of weakened wind stress. In particular, the KE-related changes in both nitrate and phosphate concentrations in GOA were reduced from year 0 to 1 in its maxima months (February–April), which again matches well with the Blob-related observed spatial patterns (Fig. 9a–d). Further, KE-related total phytoplankton content is significantly reduced in the open ocean (Fig. 9e, f) and mirrors the observed evolution during the Blob. Given that the open ocean region is the most productive oceanic region in the northeast Pacific in the winter, even a small reduction in biomass can have a significant impact on energy transfer to higher trophic levels[15,45].

Discussion and conclusion
The findings of this study provide a pathway to explore the linkages between KE variations and the occurrence of the Blob in the

Gulf of Alaska (Fig. 10). Our research here indicates that KE-influenced SLP patterns result in a ridge-like structure over the GOA (Fig. 5b, c). With regard to the influence of this ridge, it has been determined that the anticyclonic flow associated with the ridge drastically reduced the westerly flow strength limiting the energy passed from the atmosphere to the ocean, thus enhancing mixed layer stratification, decreasing cold water advection from the Bering Sea, reducing vertical entrainment of cold water from below, and limiting seasonal cooling of the upper ocean. All these observations imply the fact that the initiation of the Blob occurred due to the lack of wintertime cooling in 2013/2014. Previous research suggests that the persistence of the Blob into the 2014/2015 winter time is linked to teleconnections between the North Pacific and the weak 2014/2015 El Nino[29]. Our work further indicates the persistence of the Blob is also related to the development of a low-pressure structure a year after wintertime KE variations (Fig. 5d), which seems to have an even greater influence on warming in the region by weakening the wind stress and reducing the mixed layer thickness within the Blob region. This persistence of weakened windstress and reduced mixed layer thickness associated with KE variability corresponds well with the
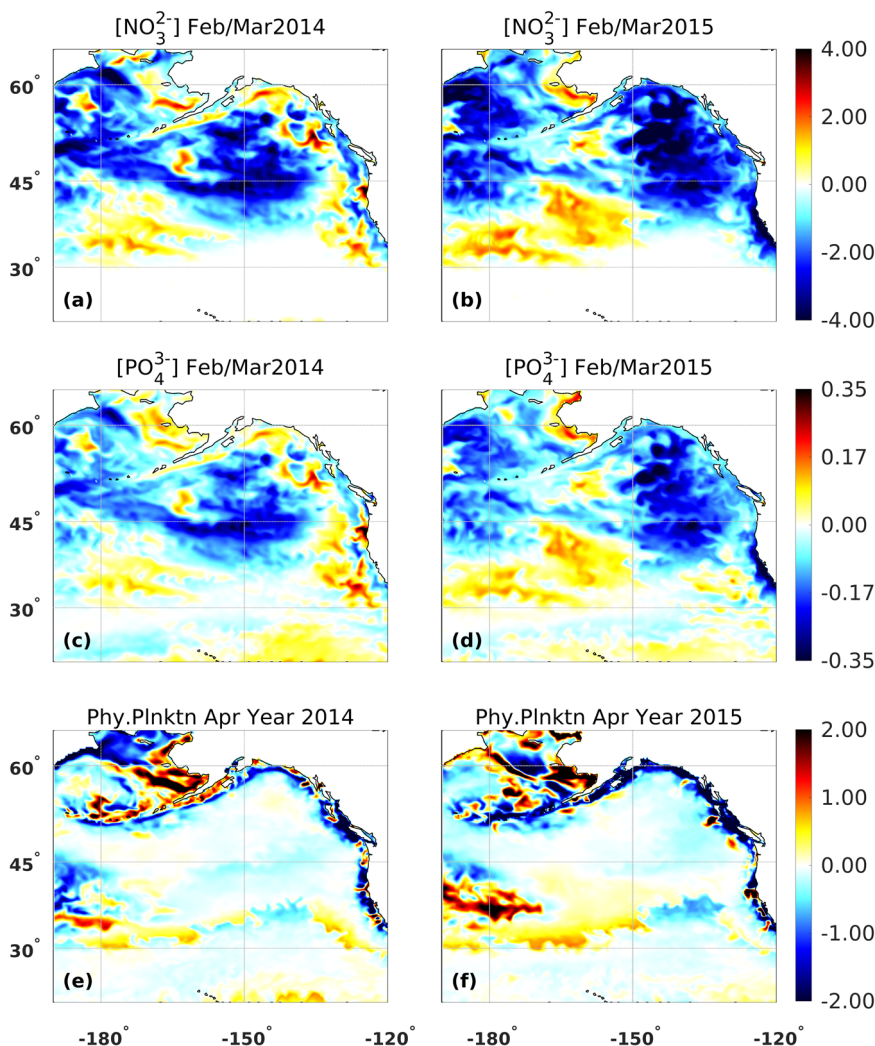
Fig. 8 Observed ocean nutrients and primary production. a, b Observed mole concentration anomalies of nitrate in seawater (NO_3^{2-}) in the Gulf of Alaska region from 2014 to 2015 spring (shading—Units: mmol m^{-3}). **c, d** Observed mole concentration anomalies of phosphate in seawater (PO_4^{3-}) in the Gulf of Alaska region from 2014 to 2015 winters (shading—Units: mmol m^{-3}). **e, f** Observed total primary production anomalies of phytoplankton in the Gulf of Alaska region from 2014 to 2015 spring (shading—Units: mg m^{-3} day^{-1}).

unusual record minima of observed windstress[9] and mixed layer depths from the 2013 to 2015 winter.

As noted in the Introduction, the Blob was followed by multiple unusual biological events in the region. These include substantial decreases in phytoplankton biomass in the region during the late winter/spring of 2014[15]. This biomass reduction has previously been linked to the anomalous winds associated with the Blob that weakened the nutrient transport into the mixed layer in the northeast Pacific. In particular, research suggests that typical winter winds from the southwest in the Northeast Pacific Transition Zone (a highly productive front in the region's open ocean—30N–40N & 180W–130W) were blocked by the high-pressure ridge in October 2013 with a continuation until January 2014. Alternatively, It has been suggested that increased ocean stratification and altered wind-driven Ekman transport and pumping modified the timing and locations of upwelling on the coast[46]; further, the stratified ocean led to a reduction in the vertical mixing that reduced the nutrient flux up to the euphotic zone, deepening the nutricline during the Blob in the Southern California Bight[47]. While our results suggest a similar blocking of nutrients as a result of KE influence in Year 0, during Year 1, the high-pressure anomaly is replaced by a low-pressure anomaly,

which in turn maintains the reduction in windstress and reduced mixed layer depths. Further, the reduction in nutrients during both years is co-located with the large variations in mixed-layer depths, particularly in Year 1 (Fig. 7d; Fig. 9b, d). This suggests that KE variations can play a role in reducing nutrients through a reduction in the vertical mixing of nutrients into the euphotic zone during the Blob. In turn, this reduced nutrient transport reduced the primary productivity. Importantly these KE-influenced reductions in nutrients and primary productivity are spatially well correlated with observed changes during the Blob, supporting our hypothesis that KE variations not only influenced the physical state of the ocean but also influenced the biological state of the ocean during the Blob.

At the same time, while the large-scale signature of primary productivity matches well with the observations and KE influence in the open ocean, the dynamics along the coast can be different and more complicated due to onshore transport and availability of iron which is a limiting factor and is largely available from river runoff along the coasts[48] which in turn is regulated by precipitation. As it turns out, one of PDP's strongest influences on the North American continent is precipitation over the Pacific Northwest[40,49]. Therefore, we hypothesize that KE-related
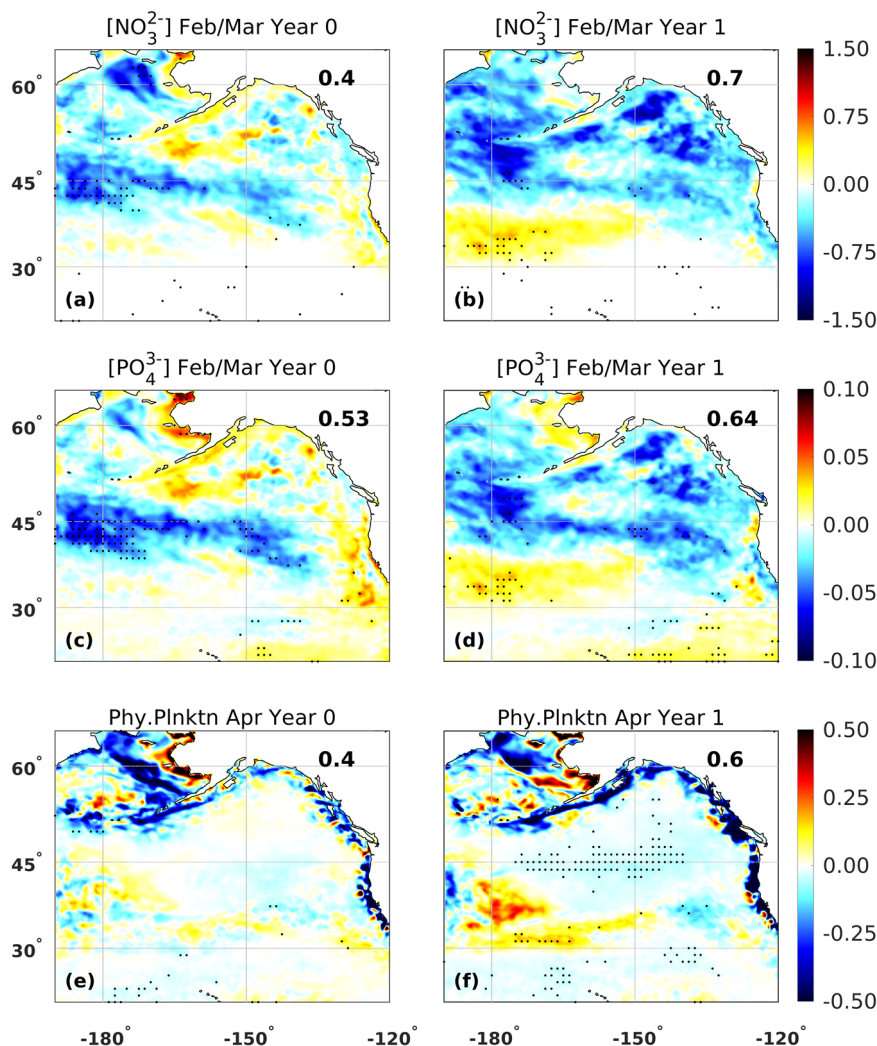
Fig. 9 KE-influenced ocean nutrients and primary production. a, b Regression coefficients of NO_3^{2-} concentration anomalies (shading—Units: mmol m^{-3}) when Feb–Mar NO_3^{2-} is regressed on KE index with no lag and NO_3^{2-} lagged by 1 year, respectively. **c, d** Regression coefficients of PO_4^{3-} concentration anomalies (shading—Units: mmol m^{-3}) when Feb–Mar PO_4^{3-} is regressed on KE index with no lag and lagged by 1 year, respectively. **e, f** Regression coefficients of total primary production anomalies (shading—Units: mg m^{-3} day^{-1}) when April primary production of phytoplankton is regressed on the KE index with no lag and primary production lagged by 1 year, respectively. The top right digit of each panel indicates the spatial correlation coefficient between regression coefficients and the corresponding Blob-related map from Fig. 8. Dotted shading designates regression coefficients that exceed the $p < 0.05$ value—see "Methods".

influence on the marine environment also extends to iron availability in the coastal region, however, this hypothesis requires further analysis to be tested.

With this synthesis, we would like to conclude this paper by stating that large-scale variations of KE influence the SST structures of the GOA region and that this influence correlates well with the recent heat event that occurred in the region. Further extending to the marine environment, the changes made to the ocean structure by KE variations influenced the nutrient availability in the region and modified primary productivity. Indeed, these relationships derived using lead/lag regression analysis point us to casual relationships between the KE and Northeast Pacific, which requires further analysis. Further, model studies suggest that global warming may lead to an intensification and/or a poleward shift of the KE extension[50–52] and may experience stronger decadal variability[53]. Finally, research must be conducted to determine how KE's future spatial, temporal, and structural modifications will eventually influence this link between KE and Northeast Pacific's marine extreme conditions.

Methods

The development of the large-scale KE index was done using an Empirical Orthogonal Function analysis (EOF) within the 30°–42°N, 140°–172°E (Fig. 1 black box) domain following the work by Silva and Anderson[42]. That study confirmed it is the second mode of large-scale KE variability that sets up a PDP-like pattern in the atmosphere. Here we used the same mode for our analysis (LS EOF2) as the KE Index. The spatial pattern of this EOF is provided in supplementary figure 3 and has an explained variance of 20%. Importantly, that study also confirmed that the KE variability does not arise from a tropical influence. February–March SST anomalies (1981–2020) in the Gulf of Alaska region were regressed on the KE index values during the November–December period to isolate the KE-influenced SST evolution within lead-lag regression maps. Then these maps were compared with observed SST anomalies. All the anomalies were calculated by removing the monthly climatology and by removing linear trends at each grid point within the domain of interest. Again, the months were selected based on the peak months of the region's seasonal climatology.
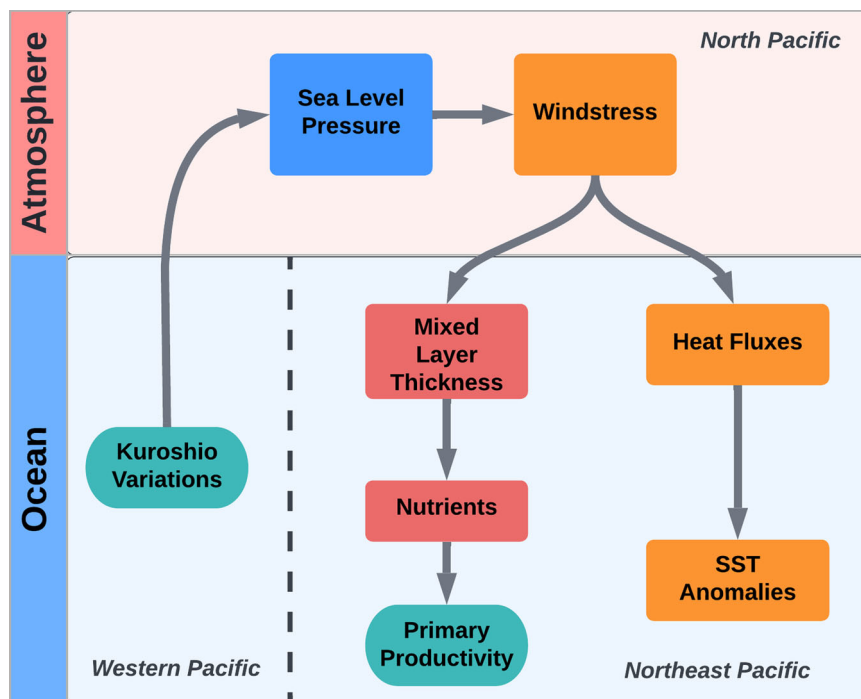
Fig. 10 Kuroshio extension and marine heatwave link. A schematic showing pathways of KE influence on the physical, chemical, and biological environment in the northeast Pacific.

To quantify the comparability between observed SSTs and lead/lag regression coefficients, we spatially correlated the regression maps with the corresponding observed SST maps. The Blob-related SST variability within the GOA region was obtained by conducting an EOF analysis, and the 2nd EOF eigenvectors were used to compare the correlation between KE and GOA SST variability. The explained variance of the GOA SST EOF1 (GOA SST EOF2) was 37% (19%). See supplementary figure 3 for the spatial patterns of GOA EOFs. To test the hypothesis that the KE influence on the Gulf of Alaska region is a teleconnection influence, we conducted a similar regression analysis to the above by using December-January sea level pressure and KE index for the November-December months (1981–2018). To further show the influence of KE-induced atmospheric pressures on the GOA ocean, we regressed December–January turbulent surface stress in the GOA region (1981–2020), January–March mixed layer thickness (1993–2020), and January–February total heat fluxes (1981–2020) on November–December KE with the same year and a 1-year lag of diagnostics considered. The rationale for selecting these particular months is based on the seasonal variability of these diagnostics (See Supplementary Fig. 4). The months we selected represent the lowest SLP, strongest wind stress, and the deepest mixed layer thickness in the region's seasonal climatology. For total heat fluxes, we selected January and February months, given these months are two of the cold season months where heat fluxes from the ocean to the atmosphere are largest (given the sign convention in which ocean heat fluxes to the atmosphere are negative). Then we quantified the KE influence with Blob-related diagnostics by conducting a spatial correlation within the Blob domain (Green box in Fig. 1) between the regression maps and observed diagnostics. To determine the influence of KE on marine nutrients and primary productivity, we repeated the same analysis using February–March nitrate and phosphate anomalies and April total phytoplankton anomalies (1993–2020).

To test the significance of our spatial regression analysis, we generated 1000 sets of random predictor values (either 39 or 27 years, depending upon the dataset used). These predictor values have the same autocorrelation as the KE index time series. Then all analyses conducted in this study were replicated using these randomized time series to determine the likelihood of our regression values arising by chance with a two-tailed significance of p-value < 0.05 as the threshold.

SST data used for this study comes from the Global Ocean Operational Sea Surface Temperature and Ice Analysis (OSTIA) reprocessed product[54] acquired through Copernicus Marine Services. This data has a spatial resolution of $0.05° \times 0.05°$ at a daily temporal resolution. For SLP, Windstress, and Total Heat-flux, we used European Center for Medium-Range Weather Forecasts fifth generation reanalysis ERA5[55] high resolution $0.25° \times 0.25°$ monthly data. MLD data were acquired from the Multi Observation Global Ocean ARMOR3D L4 analysis and multi-year reprocessing available with a $0.25° \times 0.25°$ spatial resolution at weekly or monthly intervals.

For nutrients and primary productivity data, we used model data from a biogeochemical hindcast for the global ocean that provides 3-dimensional biogeochemical fields. This hindcast uses the Pelagic Interactions Scheme for Carbon and Ecosystem Studies (PISCES) model[56], which is part of the Nucleus for European Modeling of the Ocean (NEMO) modeling platform. Daily 3D temperature, salinity, vertical turbulent diffusivity 2D MLD, and sea ice fraction from simulation FREEGLORYS2V4 have been used as the ocean and sea ice forcing on PISCES. Atmospheric forcings on PISCES, which are wind speed at 10 m, net freshwater flux into the ocean, and net shortwave solar flux, are from the ERA-interim product.

Validation/assessment for this product has been done by systematic comparison of model data with available gridded data from satellite ocean color products and World Ocean Atlas climatologies of nitrate, silicate, phosphate, and dissolved oxygen[57]. In the North Pacific region, the root mean square difference between observed and model data is 0.339 log10 $(mg\, m^{-3})$ with a bias of -0.078 log10 $(mg\, m^{-3})$. For chlorophyll climatology, the model slightly underestimates the values in the region. But for

nitrates and phosphates, the model well estimates the climatology in the Gulf of Alaska region. Further, PISCES estimates the seasonal mean chlorophyll concentration (April–June) very well in the Gulf of Alaska when compared with the satellite observations from GLOBCOLOUR[56]. The same is true for annual mean nitrate concentrations in the region.

Data availability

Code availability

References

1. Pearce, A. F. & Feng, M. The rise and fall of the "marine heat wave" off Western Australia during the summer of 2010/2011. *J. Mar. Syst.* **111–112**, 139–156 (2013).
2. Holbrook, N. J. et al. A global assessment of marine heatwaves and their drivers. *Nat. Commun.* **10**, 2624 (2019).
3. Hobday, A. J. et al. A hierarchical approach to defining marine heatwaves. *Prog. Oceanogr.* **141**, 227–238 (2016).
4. Wernberg, T. et al. An extreme climatic event alters marine ecosystem structure in a global biodiversity hotspot. *Nat. Clim. Change* **3**, 78–82 (2013).
5. Wernberg, T. et al. Climate-driven regime shift of a temperate marine ecosystem. *Science* **353**, 169–172 (2016).
6. Thomsen, M. S. et al. Local extinction of bull kelp (Durvillaea spp.) due to a marine heatwave. *Front. Mar. Sci.* **6**, 84 (2019).
7. Smale, D. A. et al. Marine heatwaves threaten global biodiversity and the provision of ecosystem services. *Nat. Clim. Change* **9**, 306–312 (2019).
8. Hughes, T. P. et al. Global warming transforms coral reef assemblages. *Nature* **556**, 492–496 (2018).
9. Bond, N. A., Cronin, M. F., Freeland, H. & Mantua, N. Causes and impacts of the 2014 warm anomaly in the NE Pacific. *Geophys. Res. Lett.* **42**, 3414–3420 (2015).
10. Smith, K. E. et al. Biological impacts of marine heatwaves. *Annu. Rev. Mar. Sci.* **15**, 119–145 (2023).
11. Oliver, E. C. J. et al. Longer and more frequent marine heatwaves over the past century. *Nat. Commun.* **9**, 1324 (2018).
12. Mills, K. E. et al. Fisheries management in a changing climate: lessons from the 2012 ocean heat wave in the Northwest Atlantic. *Oceanography* **26**, 191–195 (2013).
13. Walsh, J. E. et al. The high latitude marine heat wave of 2016 and its impacts on Alaska. *Bull. Am. Meteorol. Soc.* **99**, S39–S43 (2018).
14. Cavole, L. et al. Biological impacts of the 2013–2015 warm-water anomaly in the Northeast Pacific: winners, losers, and the future. *Oceanography* **29**, 273–285 (2016).
15. Whitney, F. A. Anomalous winter winds decrease 2014 transition zone productivity in the NE Pacific. *Geophys. Res. Lett.* **42**, 428–431 (2015).
16. Hart, L. C. et al. Abalone recruitment in low-density and aggregated populations facing climatic stress. *J. Shellfish Res.* **39**, 359 (2020).
17. Harvell, C. D. et al. Disease epidemic and a marine heat wave are associated with the continental-scale collapse of a pivotal predator (*Pycnopodia helianthoides*). *Sci. Adv.* **5**, eaau7042 (2019).
18. Peterson, W., Bond, N. & Robert, M. The blob (part three): Going, going, gone? *PICES Press* **24**, 46 (2016).
19. McKinstry, C. A. E., Campbell, R. W. & Holderied, K. Influence of the 2014–2016 marine heatwave on seasonal zooplankton community structure and abundance in the lower Cook Inlet, Alaska. *Deep Sea Res. Part II Top. Stud. Oceanogr.* **195**, 105012 (2022).
20. Sanford, E., Sones, J. L., García-Reyes, M., Goddard, J. H. R. & Largier, J. L. Widespread shifts in the coastal biota of northern California during the 2014–2016 marine heatwaves. *Sci. Rep.* **9**, 4216 (2019).
21. Opar, A. Lost at sea: starving birds in a warming world. *Audubon* https://www.audubon.org/magazine/march-april-2015/lost-sea-starving-birds-warming-world (2015).
22. NOAA. 2015–2016 Large Whale Unusual Mortality Event in the Western Gulf of Alaska, United States and British Columbia. vol. 2021 (2016).
23. Santora, J. A. et al. Habitat compression and ecosystem shifts as potential links between marine heatwave and record whale entanglements. *Nat. Commun.* **11**, 536 (2020).
24. NOAA. *California sea lion unusual mortality event in California.* (2015).
25. Moore, S. K. et al. An index of fisheries closures due to harmful algal blooms and a framework for identifying vulnerable fishing communities on the U.S. West Coast. *Mar. Policy* **110**, 103543 (2019).
26. Barbeaux, S. J., Holsman, K. & Zador, S. Marine heatwave stress test of ecosystem-based fisheries management in the Gulf of Alaska Pacific Cod Fishery. *Front. Mar. Sci.* **7**, 703 (2020).
27. Suryan, R. M. et al. Ecosystem response persists after a prolonged marine heatwave. *Sci. Rep.* **11**, 6235 (2021).
28. Amaya, D. J., Miller, A. J., Xie, S.-P. & Kosaka, Y. Physical drivers of the summer 2019 North Pacific marine heatwave. *Nat. Commun.* **11**, 1903 (2020).
29. Di Lorenzo, E. & Mantua, N. Multi-year persistence of the 2014/15 North Pacific marine heatwave. *Nat. Clim. Change* **6**, 1042–1047 (2016).
30. Peterson, W., Robert, M. & Bond, N. The warm blob—conditions in the northeastern Pacific Ocean. *PICES Press* **23**, 36–38 (2015).
31. Ren, X., Liu, W., Capotondi, A., Amaya, D. J. & Holbrook, N. J. The Pacific Decadal Oscillation modulated marine heatwaves in the Northeast Pacific during past decades. *Commun. Earth Environ.* **4**, 218 (2023).
32. Swain, D. L. et al. The Extraordinary California Drought of 2013/2014: character, context, and the role of climate. *Bull. Am. Meteorol. Soc.* **95**, S3–S7 (2014).
33. Hartmann, D. L. Pacific sea surface temperature and the winter of 2014. *Geophys. Res. Lett.* **42**, 1894–1902 (2015).
34. Wang, S. -Y., Hipps, L., Gillies, R. R. & Yoon, J. Probable causes of the abnormal ridge accompanying the 2013–2014 California drought: ENSO precursor and anthropogenic warming footprint. *Geophys. Res. Lett.* **41**, 3220–3226 (2014).
35. Lee, M., Hong, C. & Hsu, H. Compounding effects of warm sea surface temperature and reduced sea ice on the extreme circulation over the extratropical North Pacific and North America during the 2013–2014 boreal winter. *Geophys. Res. Lett.* **42**, 1612–1618 (2015).
36. Seager, R. et al. Causes of the 2011–14 California Drought*. *J. Clim.* **28**, 6997–7024 (2015).
37. Mantua, N. J., Hare, S. R., Zhang, Y., Wallace, J. M. & Francis, R. C. A Pacific Interdecadal Climate Oscillation with Impacts on Salmon Production. *Bull. Am. Meteorol. Soc.* **78**, 1069–1080 (1997).
38. Di Lorenzo, E. et al. North Pacific Gyre Oscillation links ocean climate and ecosystem change. *Geophys. Res. Lett.* **35**, L08607 (2008).
39. Joh, Y. & Di Lorenzo, E. Increasing coupling between NPGO and PDO leads to prolonged marine heatwaves in the Northeast Pacific. *Geophys. Res. Lett.* **44**, 11,663–11,671 (2017).
40. Anderson, B. T., Gianotti, D. J. S., Furtado, J. C. & Lorenzo, E. D. A decadal precession of atmospheric pressures over the North Pacific. *Geophys. Res. Lett.* **43**, 3921–3927 (2016).
41. Anderson, B. T. Empirical Evidence Linking the Pacific Decadal Precession to Kuroshio Extension Variability. *J. Geophys. Res. Atmos.* **124**, 12845–12863 (2019).
42. Silva, E. N. S. & Anderson, B. T. Influence of Kuroshio Extension Variability on the North Pacific Atmosphere and Pacific Decadal Precession. Preprint at https://doi.org/10.21203/rs.3.rs-1451566/v2 (2023).
43. Joh, Y., Di Lorenzo, E., Siqueira, L. & Kirtman, B. P. Enhanced interactions of Kuroshio Extension with tropical Pacific in a changing climate. *Sci. Rep.* **11**, 6247 (2021).
44. Sarkar, N., Royer, T. C. & Grosch, C. E. Hydrographic and mixed layer depth variability on the shelf in the northern Gulf of Alaska, 1974–1998. *Cont. Shelf Res.* **25**, 2147–2162 (2005).
45. Howard, E., Emerson, S., Bushinsky, S. & Stump, C. The role of net community production in air-sea carbon fluxes at the North Pacific subarctic-subtropical boundary region. *Limnol. Oceanogr.* **55**, 2585–2596 (2010).
46. Dewey, R. The warm pacific anomaly (The Blob): a summary on the dynamics and some recent Canadian observations. *Pacific Anomalies Workshop* (2016).
47. Zaba, K. D. & Rudnick, D. L. The 2014–2015 warming anomaly in the Southern California Current System observed by underwater gliders. *Geophys. Res. Lett.* **43**, 1241–1248 (2016).

48. Coyle, K. O., Hermann, A. J. & Hopcroft, R. R. Modeled spatial-temporal distribution of productivity, chlorophyll, iron and nitrate on the northern Gulf of Alaska shelf relative to field observations. *Deep Sea Res. Part II Top. Stud. Oceanogr.* **165**, 163–191 (2019).
49. Anderson, B. T., Gianotti, D. J. S., Salvucci, G. & Furtado, J. Dominant time scales of potentially predictable precipitation variations across the continental United States. *J. Clim.* **29**, 8881–8897 (2016).
50. Chen, C., Wang, G., Xie, S.-P. & Liu, W. Why does global warming weaken the Gulf Stream but intensify the Kuroshio? *J. Clim.* **32**, 7437–7451 (2019).
51. Nishikawa, H., Nishikawa, S., Ishizaki, H., Wakamatsu, T. & Ishikawa, Y. Detection of the Oyashio and Kuroshio fronts under the projected climate change in the 21st century. *Prog. Earth Planet. Sci.* **7**, 29 (2020).
52. Zhang, X., Wang, Q. & Mu, M. The impact of global warming on Kuroshio Extension and its southern recirculation using CMIP5 experiments with a high-resolution climate model MIROC4h. *Theor. Appl. Climatol.* **127**, 815–827 (2017).
53. Joh, Y. et al. Stronger decadal variability of the Kuroshio Extension under simulated future climate change. *Npj Clim. Atmos. Sci.* **5**, 63 (2022).
54. Donlon, C. J. et al. The operational sea surface temperature and sea ice analysis (OSTIA) system. *Remote Sens. Environ.* **116**, 140–158 (2012).
55. Hersbach, H. et al. The ERA5 global reanalysis. *Quarterly Journal of the Royal Meteorological Society* **146**, 1999–2049 (2020).
56. Aumont, O., Ethé, C., Tagliabue, A., Bopp, L. & Gehlen, M. PISCES-v2: an ocean biogeochemical model for carbon and ecosystem studies. *Geosci. Model Dev.* **8**, 2465–2513 (2015).
57. Perruche, C., Szczypta, C., Paul, J. & Drévillon, M. Quality Information Document Global Production Centre GLOBAL_REANALYSIS_BIO_001_029. (2019).

Acknowledgements

Author contributions

The study was initialized together by B.A. and E.N.S.S. E.N.S.S. conducted most of the data analysis, created the figures, and wrote the initial draft of the paper. B.A. contributed to the data analysis by providing code, interpretation of outputs, and the preparation of the paper. B.A. contributed to the commenting of the results and revising of the paper. All authors commented on the paper and discussed the results at all stages.

Competing interests

The authors declare no competing interests.

Additional information

Supplementary information The online version contains supplementary material available at https://doi.org/10.1038/s43247-023-01010-1.

Correspondence and requests for materials should be addressed to E. Nishchitha S. Silva.

Peer review information *Communications Earth & Environment* thanks Toru Miyama and the other anonymous reviewer(s) for their contribution to the peer review of this work. Primary Handling Editors: José Luis Iriarte Machuca, Heike Langenberg. A peer review file is available.

Reprints and permission information is available at http://www.nature.com/reprints

Publisher's note Springer Nature remains neutral with regard to jurisdictional claims in published maps and institutional affiliations.